Supplementary Material for the article submitted to Soft Matter entitled "Role of disclinations in determining the morphology of deformable fluid interfaces"

N. Ramakrishnan[1],* John H. Ipsen[2],† and P. B. Sunil Kumar[1,2‡]
[1] *Department of Physics, Indian Institute of Technology Madras, Chennai, India, 600036 and*
[2] *MEMPHYS- Center for Biomembrane Physics, Department of Physics and Chemistry, University of Southern Denmark, Campusvej 55, DK-5230 Odense M, Denmark*
(Dated: December 15, 2011)

PACS numbers:

I. MODEL FOR MEMBRANE SURFACE WITH IN-PLANE ORDER

A. Continuum model

Biological membranes are 2D surfaces embedded in three dimensional space. They are fluid like in the lateral direction, *ie., they flow when sheared* , while they resist deformation in the perpendicular direction, *ie., bending modes cost energy.* The equilibrium bending energy and the associated surface conformations are described by the Helfrich free energy functional[1],

$$\mathscr{H}_{\rm sur} = \int_S d\mathbf{S}\, \left\{\kappa H^2 + \sigma + \kappa_G R\right\} + \int_V \Delta p\, dV. \tag{1}$$

The curvature invariants are the mean curvature, $H = Tr(K_{ab})$, and Gaussian curvature, $R = \det(K_{ab})$, where K_{ab} is the second fundamental form known as the curvature tensor. κ, σ and κ_G are phenomenological parameters associated with membrane rigidity, surface tension and Gaussian rigidity respectively. Δp is the osmotic pressure difference.

Anisotropy arising from the presence of various internal degrees of freedom is represented by a p-atic vector field , $\vec{m}$, defined on the surface of the membrane. We will be concentrate on nematic fields, $p = 2$, throughout. The general form of the nematic field deformation energy is given by the Frank's free energy[2–4],

$$\mathscr{H}_{\rm nem} = \frac{1}{2}\oint d\mathbf{S}\left\{K_1(Div(\hat{m}))^2 + K_3(Div(\hat{m}^\perp))^2\right\}.$$

Since we are only working in the one-constant approximation: $K_A = K_1 = K_3$, we have,

$$\mathscr{H}_{\rm nem} = \frac{K_A}{2}\int_S d\mathbf{S}\, Tr(\nabla\hat{m} : \nabla\hat{m}) \tag{2}$$

K_A is the stiffness constant in the one constant approximation of the Frank's free energy for nematic field. The covariant derivative ∇ implicitly couples the nematic to the surface curvature. The elastic behaviour of the membrane is made anisotropic by explicitly coupling the surface field to the curvature tensor with interactions of the form[5],

$$\mathscr{H}_{\rm anis} = \frac{1}{2}\int_S d\mathbf{S}\left\{\kappa_\parallel\left[m^\mu K_{\mu\nu}m^\nu - C_0^\parallel\right]^2 - \kappa_\perp\left[m_\perp^\mu K_{\mu\nu}m_\perp^\nu - C_0^\perp\right]^2\right\}. \tag{3}$$

*Electronic address: ram@physics.iitm.ac.in
†Electronic address: ipsen@memphys.sdu.dk
‡Electronic address: sunil@physics.iitm.ac.in

The in-plane vector field induce directional curvatures, $C_0^{\parallel}$ and $C_0^{\perp}$, on the membrane parallel and perpendicular to its long axis. Their presence further modifies the membrane stiffness by $\kappa_{\parallel}$ and $\kappa_{\perp}$ along and normal to the nematic orientation respectively. The total energy of the membrane with an in-plane surface field is then,

$$\mathscr{H}_{\rm tot} = \mathscr{H}_{\rm sur} + \mathscr{H}_{\rm nem} + \mathscr{H}_{\rm anis} \tag{4}$$

II. DISCRETIZED MODEL

In this approach, the vesicle, a two dimensional closed surface, embedded in three dimensional space, is discretized into a set of, interconnected, self avoiding, triangular plaquettes. Each of these plaquette correspond to a flat bilayer patch of the membrane. The T plaquettes, constituting L independent links, intersect at N vertex points. The topology of the closed discretized surface, is defined by the Euler characteristics $\chi = N + T - L$, with $\chi = 2$ for a sphere.

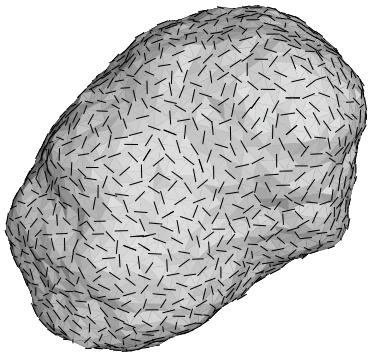

FIG. 1: (Color online) A membrane surface discretized into a triangular map with N vertices, T triangles and L links. The nematic field $\hat{m}(v)$, in an isotropic phase in the illustration, is defined as an unit vector on the tangent plane at each vertex v.

In this representation, $c_1(v)$ and $c_2(v)$ are the principal curvatures at a vertex v and $\hat{e}_1(v)$ and $\hat{e}_2(v)$ are the corresponding principal directions, see Sec:III for details. Further, the in-plane orientational order is discretized into a surface vector field $\hat{m}(v)$, of unit magnitude, defined on the tangent plane of each vertex v. In the Darboux frame, see Fig.3, $\hat{m}(v) = [\cos\varphi(v), \sin\varphi(v), 0]$, with $\varphi(v)$ being the orientation of $\hat{m}(v)$ with respect to $\hat{e}_1(v)$.

The bending energy Eq.(1), in the discretized form, is given by,

$$\mathscr{H}_{\rm sur} = \sum_{v=1}^{N} A(v) \left\{ \kappa \left[\frac{c_1(v) + c_2(v)}{2} \right]^2 + \sigma + \kappa_G \, c_1(v) c_2(v) \right\} + \Delta p V. \tag{5}$$

$A(v)$ is the area enclosed by vertex v, calculated as $A(v) = \sum_{T \in v} A(T)/3$. The summation is carried over all triangles that have v as one of its vertex and $A(T)$ is the area of the triangle T. The interaction of the nematic field, in Eq.(2), is modelled using the Lebwohl Lasher model. The corresponding Hamiltonian is,

$$\mathscr{H}_{\rm nem} = -\frac{\epsilon_{\rm LL}}{2} \sum_{\langle vv' \rangle} \left\{ \frac{3}{2} \cos^2(\varphi(v, v')) - \frac{1}{2} \right\}. \tag{6}$$

$\varphi(v, v')$ is the angle between $\hat{m}(v)$ and $\hat{m}(v')$, calculated using parallel transport technique defined in Sec.III. The anisotropic field curvature is evaluated in the local Darboux frame and has the form,

$$\mathscr{H}_{\rm anis} = \sum_{v=1}^{N} A(v) \left\{ \kappa_{\parallel} [H_{\parallel}(v) - c_0^{\parallel}]^2 + \kappa_{\perp} [H_{\perp}(v) - c_0^{\perp}]^2 \right\}. \tag{7}$$

$\kappa_\parallel$ and $\kappa_\perp$ are the directional bending rigidities parallel (or antiparallel) and perpendicular to the field $\vec{m}$. These phenomenological parameters, along with the directional spontaneous curvatures $c_0^\parallel$ and $c_0^\perp$, quantify the interaction strength of the protein with the membrane. The directional curvatures of the membrane at a vertex v, calculated using Gauss formula, are $H_\parallel(v) = c_1(v)\cos^2\varphi(v) + c_2(v)\sin^2\varphi(v)$ and $H_\perp = c_2(v)\cos^2\varphi(v) + c_1(v)\sin^2\varphi(v)$.

III. CURVATURE CALCULATION AND PARALLEL TRANSPORT OF VECTOR FIELDS

(*Reproduced from [6] for the convenience of readers*)

Contrary to the standard differential geometry of continuum models, the discretized formulation in this section is given in Cartesian coordinates. The surface is discretized by a triangulation $\mathcal{T}^N$ consisting of N vertices connected by $N_L = 3(N-2)$ links, or tethers, forming closed planar graphs. The graph form a system of $N_T = 2(N-2)$ triangles corresponding to a surface with total Euler index $\chi = N - N_T - N_L = 2$. Each vertex v takes a position $\vec{X}(v)$ in $\mathbb{R}^3$. The triangulation and the vertex position together form a discretized surface, a patch of which is given in Fig. 2(a). The self-avoidance

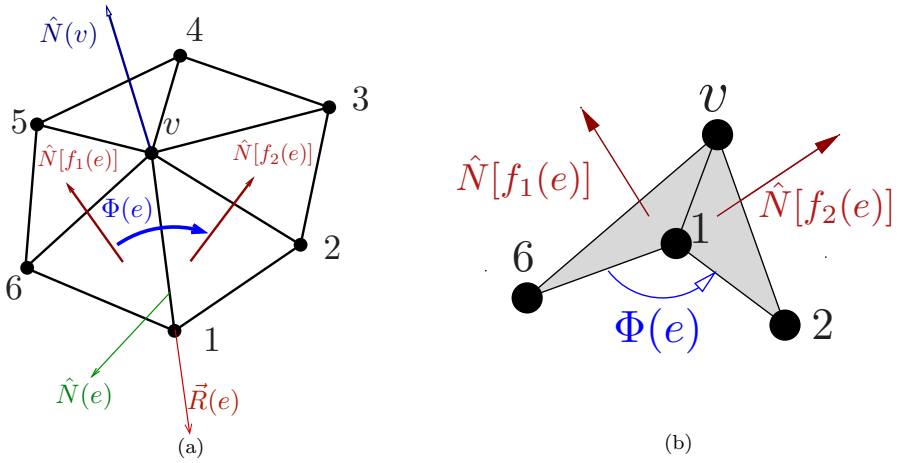

FIG. 2: (Color online) (a) A surface patch showing a one ring neighbourhood around vertex v. $\hat{N}(v)$ represents the normal to the tangent plane at v. $\vec{R}(e)$ represents the vector along an edge e, while $\hat{N}(e)$ is its normal. (b) the signed dihedral angle $\Phi(e)$ between faces, f_1 and f_2, sharing an edge e.

of the surface is ensured by assigning a hard core spherical bead of unit diameter to each vertex and a maximal tether distance of $\sqrt{3}$. This is in general not sufficient to impose strict self avoidance [7, 8], but a mild constraint on the dihedral angle between two faces sharing a tether restores self avoidance.

The in-plane orientational field can be included by defining a unit vector $\hat{m}(v)$ in the tangent plane at each vertex v. In the following we will give meaning to this statement by analysis of the local surface topography and in turn calculate the curvature tensor, principal directions and curvature invariants[9, 10]. The approach is based on the construction of the discretized "shape operator" given by the differential form $-d\hat{N}$ in the plane of the surface, which contains all information about the local surface topography. Consider a local neighborhood around a vertex v, as shown in Fig.2(a). $\vec{R}(e)$ is the edge vector that links v to a neighboring vertex. The set of edges linked to v is $\{e\}_v$, while the oriented triangles or faces with v as one of their vertex is $\{f\}_v$. The calculation of the surface quantifiers at v is restricted to the one ring neighborhood around it, which is well defined by $\{e\}_v$ and $\{f\}_v$. Similarly the set of faces sharing an edge is given by $\{f\}_e = [f_1(e), f_2(e)]$. The normal to an edge e then is defined as,

$$\hat{N}(e) = \frac{\hat{N}[f_1(e)] + \hat{N}[f_2(e)]}{\left|\hat{N}[f_1(e)] + \hat{N}[f_2(e)]\right|}, \tag{8}$$

where $\hat{N}[f_1(e)]$ and $\hat{N}[f_2(e)]$ are the unit normal vectors to faces $f_1(e)$ and $f_2(e)$ respectively.

We will now construct the shape operator at every vertex v. Toward this, we define

$$H(e) = 2\left|\vec{R}(e)\right| \cos\left(\frac{\Phi(e)}{2}\right). \tag{9}$$

which quantifies the curvature contribution along the direction mutually perpendicular to $\vec{R}(e)$ and $\hat{N}(e)$ [9, 10]. $\Phi(e)$, as illustrated in Fig.2(b), is the signed dihedral angle between the faces, $f_1(e), f_2(e)$, sharing the edge e calculated as

$$\Phi(e) = \text{sign}\left[\left\{\hat{N}[f_1(e)] \times \hat{N}[f_2(e)]\right\} \cdot \vec{R}(e)\right] \arccos\left[\hat{N}[f_1(e)] \cdot \hat{N}[f_2(e)]\right] + \pi. \tag{10}$$

The discretized "shape operator", which quantifies both the curvature and the orientation of e is thus the tensor

$$\underline{\mathbf{S_e}}(e) = H(e)\left[\hat{R}(e) \times \hat{N}(e)\right]\left[\hat{R}(e) \times \hat{N}(e)\right], \tag{11}$$

where $\hat{R}(e) = \vec{R}(e)/|\vec{R}(e)|$ is the unit vector along edge e. Having defined the shape operators, $\{\underline{\mathbf{S_e}}(e)\}$, along the edges of the vertex v, we now proceed to compute the shape operator at v. The normal to the surface at v can be calculated as,

$$\hat{N}(v) = \frac{\sum_{\{f\}_v} \Omega[A(f)]\,\hat{N}(f)}{\left|\sum_{\{f\}_v} \Omega[A(f)]\,\hat{N}(f)\right|}, \tag{12}$$

with $A(f)$ denoting the surface area of the face f and the normalized weight factor $\Omega[A(f)]$ is proportional to the area of the face. The projection operator, $\underline{\mathbf{P}}(v) = \mathbb{1} - \hat{N}(v)\hat{N}(v)$, projects $\{\underline{\mathbf{S_e}}(e)\}$ on to the tangent plane at v [9, 10]. The shape operator at the vertex v is then a weighted sum of these projections given by

$$\underline{\mathbf{S_v}}(v) = \frac{1}{A(v)} \sum_{\{e\}_v} W(e)\,\underline{\mathbf{P}}(v)^\dagger\,\underline{\mathbf{S_e}}(e)\,\underline{\mathbf{P}}(v). \tag{13}$$

$A(v) = \sum_{\{f\}_v} A(f)/3$ is the average surface area around v, while the weight factor for an edge is calculated as $W(e) = \hat{N}(v) \cdot \hat{N}(e)$. The shape operator Eq.(13) at the vertex v is expressed in coordinates of the global reference system $[\hat{x}, \hat{y}, \hat{z}]$. Notice that, by construction, the vertex normal $\hat{N}(v)$ is an eigenvector of, $\underline{\mathbf{S_v}}(v)$, corresponding to eigenvalue zero. The two other principal directions $\hat{t}_1(v)$, $\hat{t}_2(v)$, whose corresponding eigenvalues are the principal curvatures, define the tangent plane at the vertex v. A local coordinate frame called the Darboux frame $[\hat{t}_1(v), \hat{t}_2(v), \hat{N}(v)]$, see Fig.3, can then be defined at v. The transformation from the global to Darboux frame, see Fig. 3, is obtained by first applying a

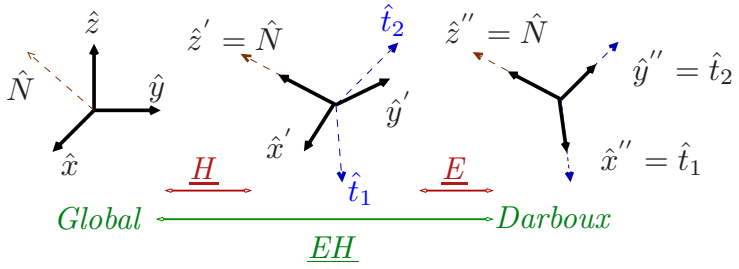

FIG. 3: (Color online) Transformation from a global to local coordinate frame.

Householder transformation($\underline{\mathbf{H}}$), see Appendix A, to rotate the global $\hat{z}$ direction into $\hat{N}(v)$, while $\hat{x}$ and $\hat{y}$ are rotated into vectors $\hat{x}', \hat{y}'$ in the tangent plane at the vertex v. The shape operator, at v, in this frame $\underline{\mathbf{C}}(v) = \underline{\mathbf{H}}^\dagger(v)\,\underline{\mathbf{S_v}}(v)\,\underline{\mathbf{H}}(v)$ is a 2x2 minor, with the two principal curvatures $c_1(v)$ and $c_2(v)$ as its

eigenvalues. The corresponding eigenvector matrix $\underline{\mathbf{E}}(v)$ transform $[\hat{x}^{'}, \hat{y}^{'}, \hat{N}(v)]$ into the Darboux frame at v. Any vector in the global frame, can now be transformed to this local frame by the transformation matrix $\underline{\mathbf{E}}(v)\,\underline{\mathbf{H}}(v)$.

We are now in the position to write up the discretized form of Helfrich's free energy, at a vertex v, based on the local curvature invariant $M(v) = [c_1(v) + c_2(v)]/2$ and $K(v) = 2c_1(v)c_2(v)$:

$$\mathscr{H}_{\rm sur} = \sum_{v=1}^{N} A(v) \left[\frac{\kappa}{2}\left(c_1(v) + c_2(v)\right)^2 + \bar{\kappa}\, c_1(v)c_2(v)\right]. \tag{14}$$

The calculation of the discrete curvature tensor has been performed by other methods [11, 12], however we find the method used in this paper to be the most accurate in describing surfaces with prescribed geometry. The local Darboux frame is very useful for the characterization of an in-plane vector field $\hat{m}(v)$. For convenience, we choose $c_1(v)$ to be the maximum principal curvature and $\hat{t}_1(v)$ the corresponding principal direction. The local orientational angle $\varphi(v)$ of $\hat{m}(v)$ will always refer to this Darboux frame. In order to compare the orientation of two distant in-plane vectors at the surface, it is necessary to perform parallel transport of the vectors on the discretized surface. In practice we need only to define the parallel transport between neighboring vertices, i.e. a transformation $\hat{m}(v^{'}) \rightarrow \underline{\mathbf{\Gamma}}(v, v^{'})\hat{m}(v)$, which brings $\hat{m}(v)$ correctly into the tangent plane of the vertex $v^{'}$, so that its angle with respect to the geodesic connecting v and $v^{'}$ is preserved. If $\hat{r}(v, v^{'})$ is the unit vector connecting a vertex v to its neighbor $v^{'}$ and $\vec{\zeta}(v)$=$\underline{\mathbf{P}}(v)\hat{r}(v, v^{'})$ and $\vec{\zeta}(v^{'})$= $\underline{\mathbf{P}}(v^{'})\hat{r}(v^{'}, v)$ are its projection on to the tangent planes at v and $v^{'}$; then our best estimate for the directions of the geodesic connecting them, are the unit vectors $\hat{\zeta}(v)$, $\hat{\zeta}(v^{'})$. The decomposition of $\hat{m}(v)$ along the orientation of the geodesic and its perpendicular in the tangent plane of v is thus:

$$\hat{m}(v) = \left[\hat{m}(v)\cdot\hat{\zeta}(v)\right]\hat{\zeta}(v) + \left[\hat{m}(v)\cdot(\hat{N}(v)\times\hat{\zeta}(v))\right]\left(\hat{N}(v)\times\hat{\zeta}(v)\right) \tag{15}$$

Parallelism now demand that these coordinates, with respect to the geodesic orientation, are the same in the tangent plane of $v^{'}$, therefore:

$$\underline{\mathbf{\Gamma}}(v, v^{'})\hat{m}(v) = \left[\hat{m}(v)\cdot\hat{\zeta}(v)\right]\hat{\zeta}(v^{'}) + \left\{\hat{m}(v)\cdot(\hat{N}(v)\times\hat{\zeta}(v))\right\}\left[\hat{N}(v^{'})\times\hat{\zeta}(v^{'})\right] \tag{16}$$

This parallel transport operation allow us to define the angle $\theta(v, v^{'})$ between vectors in the tangent plane at neighboring vertices, and in turn their cosine and sine as:

$$\begin{aligned} \cos(\varphi(v, v^{'})) &= \hat{m}(v^{'})\cdot\underline{\mathbf{\Gamma}}(v, v^{'})\hat{m}(v); \\ \sin(\varphi(v, v^{'})) &= \left[\hat{N}(v^{'})\times\hat{m}(v^{'})\right]\cdot\underline{\mathbf{\Gamma}}(v, v^{'})\hat{m}(v) \end{aligned} \tag{17}$$

We can now define the lattice models, corresponding to Eq.(2), for the in-plane orientational field, e.g., the XY-model on a random surface:

$$\mathscr{H}_{\rm XY} = -\frac{\epsilon_{\rm XY}}{2}\sum_{\langle vv^{'}\rangle}\cos[\varphi(v, v^{'})] \tag{18}$$

or the Lebwohl-Lasher model on a random surface:

$$\mathscr{H}_{\rm LL} = -\frac{\epsilon_{\rm LL}}{2}\sum_{\langle vv^{'}\rangle}\left\{\frac{3}{2}\cos^2(\varphi(v, v^{'})) - \frac{1}{2}\right\} \tag{19}$$

Furthermore, we are now in a position to calculate, at a given vertex v, the directional curvatures along and perpendicular to the orientation of the in plane vector field $\hat{n}(v)$ by use of Gauss formula:

$$\begin{aligned} H(v)_{\parallel} &= c_1(v)\cos^2[\varphi(v)] + c_2(v)\sin^2[\varphi(v)] \\ H(v)_{\perp} &= c_1(v)\sin^2[\varphi(v)] + c_2(v)\cos^2[\varphi(v)] \end{aligned} \tag{20}$$

IV. MONTE CARLO PROCEDURE

(*Reproduced from [6] for the convenience of readers*)

The equilibrium properties of the discretized surface can now be evaluated from the analysis of the total partition function, i.e., the sum of Boltzmann factors for all surface configurations and triangulations. For simplicity, we consider the situation with just one in-plane orientational $\hat{m}(v)$ field defined at each vertex

$$Z(N,\kappa,\bar{\kappa},\epsilon,..) = \frac{1}{N!}\sum_{\mathcal{T}^N}\prod_{v=1}^{N}\int d\vec{X}(v)\int d\varphi(v)\exp\left(-\beta\left(\mathscr{H}^c(\{\vec{X}\},\mathcal{T}^N,\{\varphi\})+U_{SAS}\right)\right) \tag{21}$$

where U_{SAS} is the potential that ensures the self-avoidance of the surface and $\varphi(v)$ is integrated over the unit circle or half unit circle for the XY field and the nematic field respectively. $\{\vec{X}\}$ and $\{\varphi\}$ are, respectively, the complete set of vertex positions and orientational angles. Further, we set $\beta = \frac{1}{k_B T} = 1$. In practice, a surface configuration is represented by a tuple $\eta = (\{\vec{X}\},\mathcal{T}^N,\{\varphi\})$, which must be updated during the Monte Carlo simulation procedure. The Monte Carlo updating scheme can now be decomposed into three move classes, so each of the three sets of degrees of freedom are updated independently to keep it simple and ensure fulfillment of detailed balance:

Vertex shifts: represent the updates of the vertex positions, keeping $\mathcal{T}^N,\{\varphi\}$ fixed, thus allowing for shape changes of the membrane. The attempt probability to change to a new configuration $\eta' = (\{\vec{X}'\},\mathcal{T}^N,\{\varphi\})$, with a chosen vertex moved to a new position within a cube of side 2σ centered around its old position, is $\omega(\eta|\eta') = \omega(\eta'|\eta) = ([2\sigma]^3 N)^{-1}$. σ is appropriately chosen to get a reasonable acceptance rate of 30–50%. In our simulations $\sigma = 0.1$ is chosen.With this surface updating operation, the curvature tensor and thus the principal axis changes. Since the angle $\{\varphi\}$ is kept fixed, the set of orientations $\{\hat{m}\}$, in the global frame, are changed following the local surface configuration, Fig. 4(a).

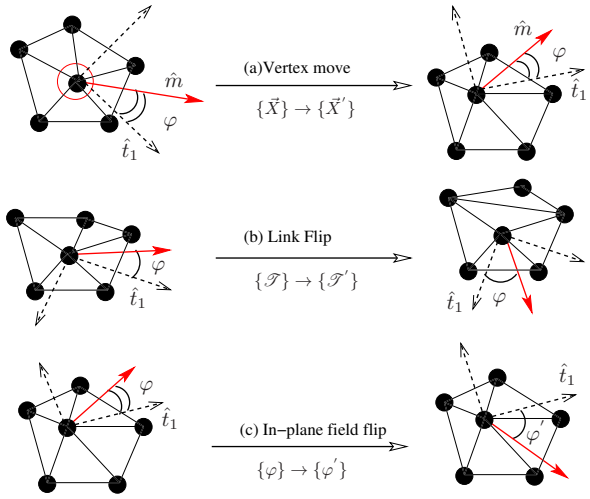

FIG. 4: Monte Carlo moves, a) vertex shift, b) link flip and c) angle rotation. Surface vector field, $\hat{m}$, is represented with solid arrow while principal directions $\hat{e}_1$ and $\hat{e}_2$ are marked with dotted arrows. φ is the angle $\hat{m}$ subtends with $\hat{e}_1$.

Link flip: represents updating of the triangulation. Here a link, e connecting a vertex v to v', is picked at random and an attempt is made to flip it to the pair of opposite vertices common to v and v'. The attempt probability to change to configuration $\eta' = (\{\vec{X}\},\mathcal{T}'^N,\{\varphi\})$ is then $\omega(\eta|\eta') = \omega(\eta'|\eta) = 1/N_L$. Similar to vertex shifts, the actual orientations $\{\hat{m}\}$ are now changed, following the local surface configuration, Fig. 4(b).

Angle rotation: the orientation of the in-plane vector $\hat{m}(v)$, at a randomly chosen vertex v, is updated. The vector is rotated to a new, randomly chosen, direction in the tangent plane, keeping the vertex positions and link directions fixed. As a result of which the orientational angle is now $\varphi^{'}(v) = \varphi(v) + \Delta\varphi(v)$. The attempt probability to configuration $\eta' = (\{\vec{X}\}, \mathcal{T}^N, \{\varphi^{'}\})$ is $\omega(\eta|\eta^{'}) = \omega(\eta'|\eta) = (2\sigma_\varphi N)^{-1}$, where $\sigma_\varphi \ll \pi$ is the maximum increment of the angle. The surface topography is not affected by this move, Fig. 4(c).

For each of the above moves, the acceptance probability is:

$$acc(\eta|\eta') = \min(1, \frac{\omega(\eta^{'}|\eta)}{\omega(\eta|\eta^{'})} \exp(-\beta \left(H(\eta^{'}) - H(\eta)\right)) \tag{22}$$

The duration of a Monte Carlo simulation is measured in MCS (Monte Carlo sweeps per Site), which represents N attempted *vertex moves*, $3(N-2)$ attempted *flips* and N attempted rotations of $\hat{n}$.

V. CONFORMATIONAL DIAGRAM IN $C_0^{\|}$ SPACE

A high resolution version of Fig.1 in the manuscript is presented here. The nematic field remodels a spherical membrane into tubes and branched structures for $C_0^{\|} > 0$, while tubes, discs and caveola like structures are seen for $C_0^{\|} < 0$

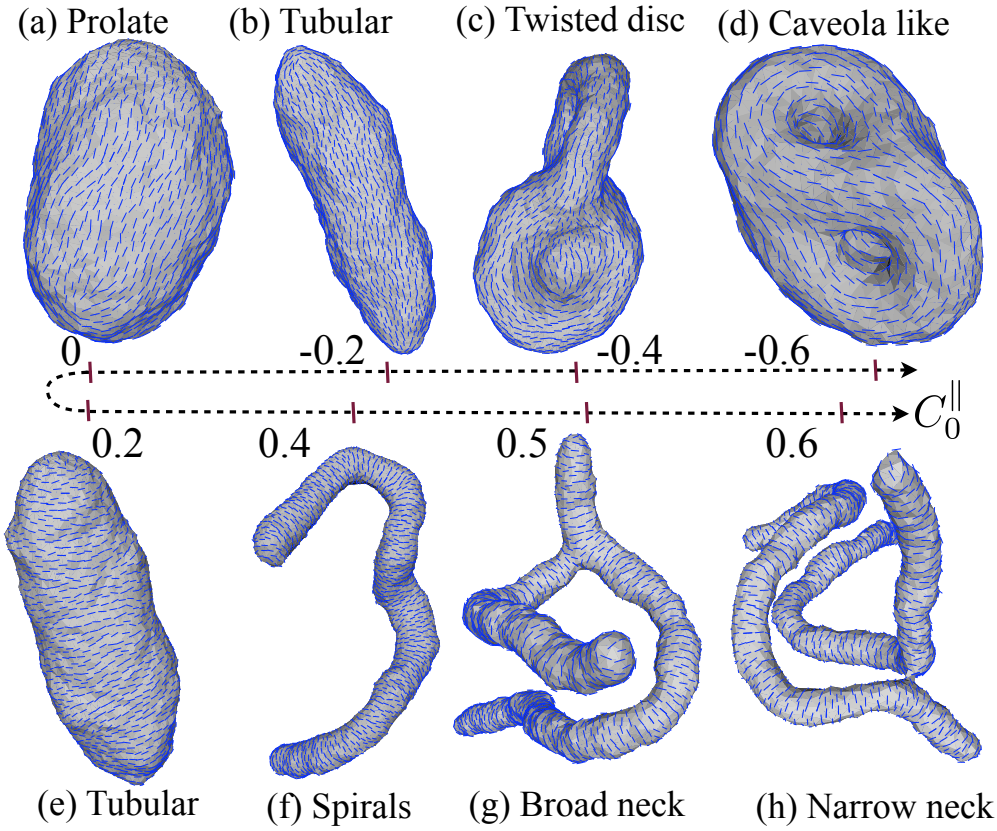

FIG. 5: High resolution version of Fig.1 in the manuscript. Two +1/2 disclination pair at the end caps of a tube while they repel each other in case of a non tubular structures, eg. in case of the disc like conformation. The parameter values are $\kappa = 10$, $\epsilon_{\rm LL} = 3$, $\kappa_{\|} = 5$ and $\kappa_{\perp} = 0$.

VI. DISCLINATIONS AND THEIR SPATIAL ORGANIZATION.

An in-plane vector field, frustrated by the spherical topology of the surface, will have orientational singularities (disclinations) in its ground state. The sum of the topological charge of these disclinations on a spherical surface is equal to the two. As, for a nematic field, the energy of a disclination is proportional to the square its charge, four disclinations, each of strength +1/2, will be present, on a surface of spherical topology, at the ground state.

A. Types of disclinations

In the study reported here, we only observe disclinations of strength +1/2 and -1/2 as in Fig.6(a) & 6(b) respectively, which are illustrated in the figure below.

(a) (b)

FIG. 6: (a) +1/2 disclination and (b) -1/2 disclination proliferated at low values of $\epsilon_{\rm LL}$ or at high values of $C_0^{\parallel}$.

B. Localization of disclinations

The interaction between disclinations are modified by the Gaussian curvature of the surface[13]. The localization of the defects depends on the morphology of the surface. When $\kappa_{\parallel} = \kappa_{\perp} = 0$, the defect cores repel each other and position themselves on the vertices of a tetrahedron.

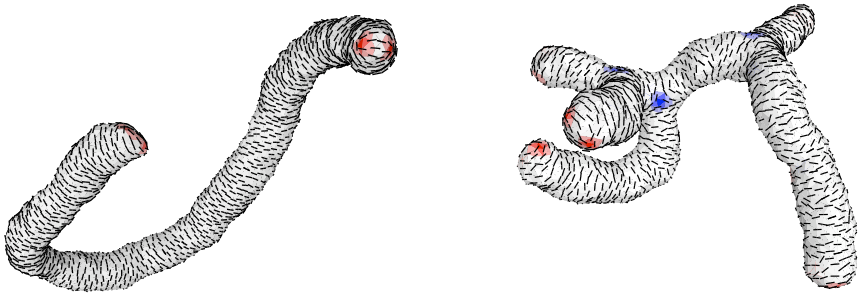

(a) (b)

FIG. 7: (a) The membrane deforms into a tube for $\kappa_{\parallel} = 5$ and $C_0^{\parallel} = 0.4$ and $\epsilon_{\rm LL} = 3$. Two +1/2 defects move towards each other and pair at the end caps while the defect pairs move away from each other. (b) Branched tubular membrane for $\kappa_{\parallel} = 5$ and $C_0^{\parallel} = 0.4$ and $\epsilon_{\rm LL} = 1$. The intersection of a branch is stabilized by two -1/2 disclinations in the negative Gaussian curvature region around the junction.

In presence of a directional bending modulus, the membrane tubulates leading to pairing of two +1/2 defects at its end cap. The repulsion between these positive disclinations is screened by the positive Gaussian curvature of the end cap (see Fig.7(a)). Negative defects, appearing through spontaneous

defect pair creation, stabilizes branched membrane conformations, by locating themselves at the negative gaussian curvature regions at the junction, as shown in Fig.7(b).

VII. MECHANISMS OF TUBULATION AND BRANCHING

When the thermal fluctuations are weak or when the nematic coupling is strong, it is unfavorable to create defect pairs, discussed earlier. In such cases, there is an effective repulsion between the defect pairs at the end caps of a tube due to the formation of tubular sections favored by the spontaneous directional curvature.

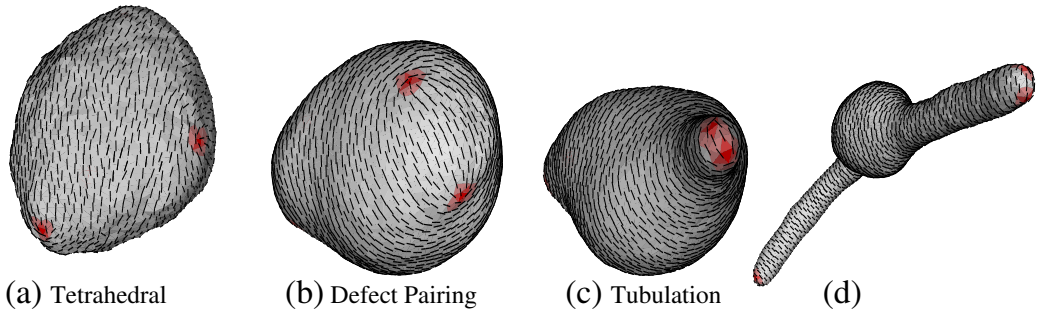

FIG. 8: Vesicle morphogenesis into a tube and the effective repulsion between defect pairs at the end caps. Shown are membrane shapes for $\kappa = 10k_BT$, $J_2 = 3k_BT$, $\kappa_\parallel = 5k_BT$, $C_0^\parallel = 0.4$ and $\beta = 1/k_BT = 5$.

A. Stabilization of branched shapes

Here we look at the case of branching of tubes. The negative defects, resulting from the thermally induced defect pair creation, move towards region of negative Gaussian curvature in Fig.9(c).

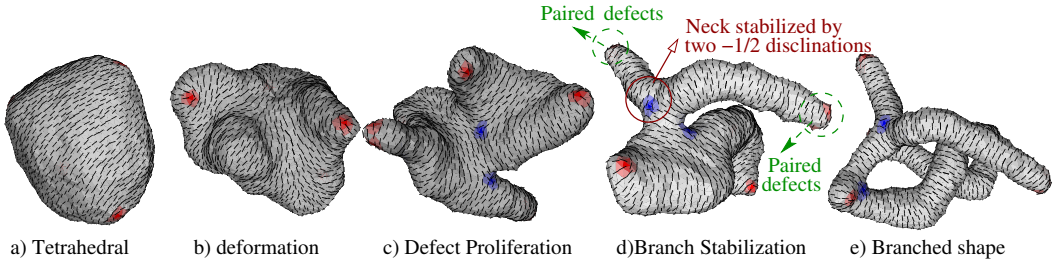

FIG. 9: Defect proliferation and stabilization of junctions by two -1/2 defects.

The $-1/2$ defects are attracted to regions with negative gaussian curvature. When two -1/2 defects reach a junction, they stabilize the branch. as in Fig.9(d). The unpaired -1/2 defects continue to remodel the membrane till its forms a junction with another -1/2 defect or annihilates with a $+1/2$ defect. A pair of $+1/2$ and -1/2 disclinations about to annihilate is shown in the leftmost branch of Fig.9(e). If $N_{\rm mhalf}$ is the number of -1/2 disclinations proliferated, the criterion for branching is $N_{\rm mhalf} \geq 2$.

VIII. STABILITY OF TUBULAR MEMBRANES WITH NEMATIC ORDER

In this supplementary section we work out the free energy expression for a general fluid tubular membrane of uniform radius with nematic ordered membrane inclusions. The starting point for the evaluation is

the general curvature free energy form for a fluid membrane equipped with nematic inclusions:

$$\mathscr{H}_{\rm tot} = \oint dA \left(\frac{\kappa}{2}(2H)^2 + \frac{\kappa_\parallel}{2}(H_\parallel - C_0^\parallel)^2 + \frac{\kappa_\perp}{2}(H_\perp - C_0^\perp)^2 \right) + \mathscr{H}_{\rm nem},$$

where, the in-plane elastic free energy of the nematic ordering field has the form

$$\mathscr{H}_{\rm nem} = \frac{K_A}{2} \oint dA \, {\rm Tr} \left(\nabla \hat{m} : \nabla \hat{m} \right). \tag{23}$$

First, we consider a cylindrical membrane with nematic order. The free energy per tube length takes the simple form:

$$f_{\rm cyl} = 2\pi r \left(\kappa_\parallel (x/r - C_0^\parallel)^2 + \kappa_\perp ((1-x)/r - C_0^\perp)^2 \right) + 2\kappa\pi/r \tag{24}$$

where r is the tube radius, $x = \cos^2(\varphi)$ is representing the orientation of the nematic field in the Darboux frame, which just follow the cylinder axis and the surface tangent perpendicular to it with principal curvatures 0 and $1/r$. For a perfect nematic order, the minimum free energy configuration obey the stationary condition, $\frac{\partial f_{\rm cyl}}{\partial x} = 0$, $\frac{\partial f_{\rm cyl}}{\partial r} = 0$

$$\bar{r} = \sqrt{\frac{\left(\frac{\kappa}{2}\right)\left(\kappa_\parallel + \kappa_\perp\right) + \kappa_\perp \kappa_\parallel}{\kappa_\perp \kappa_\parallel \left(C_0^\parallel + C_0^\perp\right)^2}} \tag{25}$$

$$\bar{x} = \cos^2(\bar{\varphi}) = \frac{\left(\kappa_\parallel C_0^\parallel - \kappa_\perp C_0^\perp\right)\bar{r} + \kappa_\perp}{\kappa_\perp + \kappa_\parallel} \tag{26}$$

Note that the above expressions are for the general case of $\kappa_\perp \neq 0, \kappa_\parallel \neq 0$ and $x = 1$ when $\kappa_\perp = 0$ and $x = 0$ when $\kappa_\parallel = 0$. So, in general both $\bar{\varphi}$ and $\bar{r}$ are set by the model parameters. Eqn.(23) is the only part of the free energy, which depends on the orientation of the nematogens. Perfect nematic order means that the nematic orientation will follow the geodesic lines on the cylinder. A well-known result from surface differential geometry that the geodesic lines on a cylinder in general are lines paralel to the long axis, circles perpendicular to the long axis or helical spirals, which are characterized by a fixed angle between the curve and the long axis of the helix (the first principal direction of the cylinder). The mean-field solution above precisely corresponds to that situation. In general, increasing κ leads to increasing radius $\bar{r}$, while increasing $C_0^\parallel$ and $C_0^\perp$ leads to decreasing radius. Another important point is to ensure that the stationary solution found is a stable solution, i.e. the second derivative of f is positive definite for the solution.

$$\begin{pmatrix} \frac{\partial^2 f}{\partial^2 x} & \frac{\partial^2 f}{\partial x \partial r} \\ \frac{\partial^2 f}{\partial r \partial x} & \frac{\partial^2 f}{\partial^2 r} \end{pmatrix}_{\bar{x},\bar{r}} = \frac{4\pi}{\bar{r}^3} \begin{pmatrix} (\kappa_\parallel + \kappa_\perp)\bar{r}^2 & -(\kappa_\parallel \bar{x} - \kappa_\perp + \kappa_\perp x)\bar{r} \\ -(\kappa_\parallel \bar{x} - \kappa_\perp + \kappa_\perp \bar{x})\bar{r} & \kappa_\parallel \bar{x}^2 + \kappa_\perp (1-\bar{x})^2 + \frac{\kappa}{2} \end{pmatrix} \tag{27}$$

Since the elastic moduli are all positive (or zero) this stability matrix positive definite for all parameter values with $\bar{r} > 0$.In the following we would like to investigate if the above observations can be generalized to include curved tubular surfaces as the results from computer simulations indicate. General tubular surfaces are also called canal surfaces and first we remind about some general nomenclature for curves and surfaces which is relevant for the analysis of canal surfaces.

Canal surfaces

In the following we will introduce a class of surfaces, which is developed by a circle of radius r, with center along a general space curve $\vec{x}_C(s)$, and oriented in the normal plane of the curve. It is called a canal surface with constant radius and spine curve $\mathcal{C}$, with s being the arc length along this curve. The Frenet frame is a good starting point for the parameterization of the surface. With $\vec{t}(s), \vec{p}(s), \vec{b}(s)$ being the unit tangent, normal and binormal to the curve.

$$\vec{x}(s,\theta) = \vec{x}_C(s) + r\left(\cos\theta\,\vec{p}(s) + \sin\theta\,\vec{b}(s)\right) \tag{28}$$

$$\partial_s\vec{x} = (1-\lambda r\cos\theta)\;\vec{t}(s) + \tau r\cos\theta\,\vec{b}(s) - \tau r\sin\theta\,\vec{p}(s) \tag{29}$$

$$\partial_\theta\vec{x} = r\left(-\sin\theta\,\vec{p}(s) + \cos\theta\,\vec{b}(s)\right) \tag{30}$$

The basic intrinsic and extrinsic geometrical quantifiers can easily be established, for such canal surfaces with constant curvature λ and torsion τ.
The metric , the mean curvature and the Gaussian curvature then have the forms:

$$g = r^2\,(1-\lambda r\cos\theta)^2 \quad H = \frac{2\lambda r\cos\theta - 1}{2r(1-\lambda r\cos\theta)} \quad \text{and} \quad G = \frac{-\lambda\cos\theta}{r(1-\lambda r\cos\theta)} \tag{31}$$

The curvature free energy: We are now in the position to calculate the free energy Eq.(1) of a helical canal surface. We will consider each contribution separately. First, the usual Helfrich term:

$$\mathscr{H}_{\rm sur} = \frac{\kappa}{2}\int\sqrt{g}\,ds\,d\theta\,(2H)^2 = \frac{\kappa}{2}\int_0^L ds\int_0^{2\pi}\frac{(1-2r\lambda\cos\theta)^2}{r(1-\lambda r\cos\theta)} = \frac{\kappa}{2}\frac{L}{r}\frac{2\pi}{\sqrt{1-(\lambda r)^2}} \tag{32}$$

The expression Eq.(32) is very similar to the Helfrich free energy of a torus. Again, we can note an expression for a helical canal surface, where the spine curve torsion do not enter. It is also follows that for a given spine curve curvature λ this functional is minimal for $\lambda r = \frac{1}{\sqrt{2}}$, which is just the condition for a Clifford torus. Finaly, it is observed that the Gaussian curvature integrate up to zero over the surface as expected.
Let us now continue with the terms involving directional curvature elasticity. First, the directional curvature for a nematogen oriented with an angle φ with respect to the Darboux frame. With $x = \cos^2(\varphi)$ and Euler's relations they become:

$$H_\parallel = \frac{x}{r} - \frac{(1-x)\lambda\cos\theta}{(1-\lambda r\cos\theta)} \qquad \text{and} \qquad H_\perp = \frac{1-x}{r} - \frac{x\lambda\cos\theta}{(1-\lambda r\cos\theta)} \tag{33}$$

The remaining curvature elastic terms are:

$$\begin{aligned}\mathscr{H}^{\parallel}_{\rm anis} &= \frac{\kappa_\parallel}{2}\int dA(H_\parallel - C_0^\parallel)^2 = \frac{\kappa_\parallel}{2}\int_0^L rds\int_0^{2\pi}d\theta\,\frac{\left\{\left(\frac{x}{r}-C_0^\parallel\right)+\lambda\cos\theta\left(rC_0^\parallel-1\right)\right\}^2}{(1-\lambda r\cos\theta)}\\ &= \frac{\kappa_\parallel}{2}\,\frac{2\pi Lr}{\sqrt{1-(\lambda r)^2}}\left(\frac{1-x}{r}\right)^2 + \frac{\kappa_\parallel}{2}\,2\pi Lr\left(\frac{1}{r}-C_0^\parallel\right)\left(\frac{2x-1}{r}-C_0^\parallel\right)\end{aligned} \tag{34}$$

and

$$\begin{aligned}\mathscr{H}^{\perp}_{\rm anis} &= \frac{\kappa_\perp}{2}\int dA\left(H_\perp - C_0^\perp\right)^2 = \frac{\kappa_\perp}{2}\int_0^L rds\int_0^{2\pi}d\theta\,\frac{\left\{(1-x-rC_0^\perp)+\lambda r\cos\theta(rC_0^\perp-1)\right\}^2}{r(1-\lambda r\cos\theta)}\\ &= \frac{\kappa_\perp}{2}\,\frac{2\pi Lr}{\sqrt{1-(\lambda r)^2}}\left(\frac{x}{r}\right)^2 + \frac{\kappa_\perp}{2}\,2\pi Lr\left(\frac{1}{r}-C_0^\perp\right)\left(\frac{1-2x}{r}-C_0^\perp\right)\end{aligned} \tag{35}$$

The nematic term:

Now, we can focus on the nematic term, defined in Eqn.(23)

$$\begin{aligned}\mathscr{H}_{\rm nem} &= \frac{K_A}{2}\int d^2\xi\sqrt{g}\,{\rm Tr}\,(\nabla\hat{m}:\nabla\hat{m})\\ &= \frac{K_A}{2}\int d^2\xi\sqrt{g}\,g^{\nu\mu}\left(\partial_\nu\hat{m}-\hat{N}(\hat{N}\partial_\nu\hat{m})\right)\left(\partial_\mu\hat{m}-\hat{N}(\hat{N}\partial_\mu\hat{m})\right)\\ &= \frac{K_A}{2}\int d^2\xi\sqrt{g}g^{\nu\mu}\left(\partial_\nu\varphi-A_\nu\right)\left(\partial_\mu\varphi-A_\mu\right)\end{aligned} \tag{36}$$

$\hat{m}$ can here be chosen in any local orthonormal coordinate system:

$$\hat{m}=\cos(\varphi)\hat{e}_1+\sin(\varphi)\hat{e}_2 \tag{37}$$

It is a natural choice for us to use the principal directions for the curvature tensor: $\hat{e}_2=\hat{t}$ and $\hat{e}_1=\hat{e}_\theta$. We can now work out some of the ingrdients in Eq(36). First we remember that

$$\hat{e}_1=\frac{\partial\hat{N}}{\partial\theta}=-\sin(\varphi)\,\hat{p}+\cos(\varphi)\,\hat{b},\qquad \hat{e}_2=\hat{t} \tag{38}$$

The geometric vector potential $A_\nu=\hat{e}_1\partial_\nu\hat{e}_2$ takes in this basis the form:

$$A_\theta=\hat{e}_1\partial_\theta\hat{t}=0,\qquad A_s=\hat{e}_1\partial_s\hat{t}=-\lambda\sin\theta \tag{39}$$

$$\begin{aligned}\mathscr{H}_{\rm nem} &= \frac{K_A}{2}\int d\theta\,ds\frac{1}{r(1-\lambda r\cos\theta)}\\ &\left\{\left[(1-\lambda r\cos\theta)^2+(r\tau)^2\right](\partial_\theta\varphi)^2+r^2(\partial_s\varphi+\lambda\sin\theta)^2-2\tau r^2\partial_s\varphi\partial_\theta\varphi-\tau r^2\lambda\sin\theta\partial_\theta\varphi)\right\}\end{aligned} \tag{40}$$

For the ansatz $\varphi=\varphi_0$, the free energy becomes:

$$\mathscr{H}_{\rm nem}=\frac{K_A}{2}\frac{2\pi rL}{\sqrt{1-(\lambda r)^2}}\left(\lambda^2-\lambda^2\frac{1-\sqrt{1-(\lambda r)^2}}{(\lambda r)^2}\right)=\frac{K_A}{2}\frac{2\pi L}{r}\left(1-\sqrt{1-(\lambda r)^2}\right). \tag{41}$$

We can put together the elastic free energy from the curvature contributions and the nematic contributions to the free energy.

$$\begin{aligned}\mathscr{H}_{\rm tot} &= \mathscr{H}_{\rm nem}+\mathscr{H}_{\rm sur}+\mathscr{H}^{\parallel}_{\rm anis}+\mathscr{H}^{\perp}_{\rm anis}\\ &= \frac{2\pi L}{r}\frac{K_A}{2}\left\{1-\sqrt{1-(\lambda r)^2}\right\}+\frac{2\pi L}{r}\left\{\frac{\frac{\kappa}{2}+\frac{\kappa_\parallel}{2}(1-x)^2+\frac{\kappa_\perp}{2}x^2}{\sqrt{1-\{\lambda r)^2}}\right\}\\ &+ \frac{2\pi L}{r}\left\{\frac{\kappa_\parallel}{2}(1-rC_0^\parallel)(2x-1-rC_0^\parallel)+\frac{\kappa_\perp}{2}(1-rC_0^\perp)(1-2x-rC_0^\perp)\right\}\end{aligned} \tag{42}$$

A simple stability analysis of the total free energy show that the elastic free energies actually are minimal for $\lambda=0$, which corresponds to the cylinder solution discussed in the beginning. The stability matrix Eqn.(27) is thus extended with one positive diagonal term :

$$\frac{1}{L}\begin{pmatrix} \frac{\partial^2 \mathscr{H}_{\rm tot}}{\partial^2 x} & \frac{\partial^2 \mathscr{H}_{\rm tot}}{\partial x \partial r} & \frac{\partial^2 \mathscr{H}_{\rm tot}}{\partial x \partial \lambda} \\ \frac{\partial^2 \mathscr{H}_{\rm tot}}{\partial r \partial x} & \frac{\partial^2 \mathscr{H}_{\rm tot}}{\partial r^2} & \frac{\partial^2 \mathscr{H}_{\rm tot}}{\partial r \partial \lambda} \\ \frac{\partial^2 \mathscr{H}_{\rm tot}}{\partial \lambda \partial x} & \frac{\partial^2 \mathscr{H}_{\rm tot}}{\partial \lambda \partial r} & \frac{\partial^2 \mathscr{H}_{\rm tot}}{\partial \lambda^2} \end{pmatrix}_{\bar{x},\bar{r},\lambda=0} =$$

$$\frac{4\pi}{\bar{r}^3}\begin{pmatrix} (\kappa_\parallel+\kappa_\perp)\bar{r}^2 & -(\kappa_\parallel\bar{x}-\kappa_\perp+\kappa_\perp x)\bar{r} & 0 \\ -(\kappa_\parallel\bar{x}-\kappa_\perp+\kappa_\perp\bar{x})\bar{r} & \kappa_\parallel\bar{x}^2+\kappa_\perp(1-\bar{x})^2+\frac{\kappa}{2} & 0 \\ 0 & 0 & \left(K_A+\kappa+\kappa_\parallel(1-\bar{x})^2+\kappa_\perp\bar{x}^2\right)\frac{\bar{r}^4}{4} \end{pmatrix} \tag{43}$$

The entropy of a spiral:

The form Eqn.(42) also shows that the free energy only depends on the curvature of the spine curve, while the torsion does not appear in the expression. Therefore, for $\lambda \neq 0$ there is a degeneracy of spiral configurations corresponding to different torsions. This deformation can e.g. be parametrized by the length of the helix along the helical axis $L_z = L\sqrt{1-\lambda R}$. The involved entropy is thus of order $k_B T \ln(\frac{L}{a})$, where a is the fundamental "microscopic" length scale in the problem. For finite tubes with sufficiently small curvatures λ the curvature elastic energy of the spine curve $\frac{1}{2}\pi L\bar{r}\left(K_A+\kappa+\kappa_\parallel(1-\bar{x})^2+\kappa_\perp\bar{x}^2\right)\lambda^2$ may be smaller than the entropy, thus favouring curved, spiral configurations.

[1] W. Helfrich, Z. Naturforsch. **28c**, 693 (1973).
[2] P. G. De Gennes and J. Prost, *The Physics of Liquid Crystals*, *The International Series of Monographs on Physics* (Clarendon Press, Oxford, 1993).
[3] P. M. Chaikin and T. C. Lubensky, *Principles of Condensed Matter Physics*, 1st ed. (Cambridge University Press, Cambridge, 2000).
[4] *Statistical Mechanics of Membranes and Surfaces*, 2nd ed., edited by D. Nelson, T. Piran, and S. Weinberg (World Scientific, Singapore, 2003).
[5] J. R. Frank and M. Kardar, Phys. Rev. E **77**, 41705 (2008).
[6] N. Ramakrishnan, P. B. S. Kumar, and J. H. Ipsen, Phys. Rev. E **81**, 41922 (2010).
[7] J. H. Ipsen and C. Jeppesen, J.Phys.I France **5**, 1563 (1995).
[8] J. S. Ho and A. Baungartner, Europhys. Lett. **12**, 295 (1990).
[9] K. Hildebrandt and K. Polthier, EUROGRAPHICS **23**, 1 (2004).
[10] K. Hildebrandt, K. Polthier, and M. Wardetzky, Eurographics Symposium on Geometry Processing 1 (2005).
[11] G.Taubin, Proc.Int.Conf.Comp.Vision (1995).
[12] E. Hameiri and I. Shimsoni, IEEE transactions on systems man and cybernetics : Cybernetics **33**, 626 (2003).
[13] M. Bowick and L. Giomi, Advances in Physics **58**, 449 (2009).